NJC

Accepted Manuscript

This is an *Accepted Manuscript*, which has been through the Royal Society of Chemistry peer review process and has been accepted for publication.

Accepted Manuscripts are published online shortly after acceptance, before technical editing, formatting and proof reading. Using this free service, authors can make their results available to the community, in citable form, before we publish the edited article. We will replace this *Accepted Manuscript* with the edited and formatted *Advance Article* as soon as it is available.

You can find more information about *Accepted Manuscripts* in the Information for Authors.

Please note that technical editing may introduce minor changes to the text and/or graphics, which may alter content. The journal's standard Terms & Conditions and the Ethical guidelines still apply. In no event shall the Royal Society of Chemistry be held responsible for any errors or omissions in this *Accepted Manuscript* or any consequences arising from the use of any information it contains.

ROYAL SOCIETY OF CHEMISTRY

www.rsc.org/njc

Development of a Fe_3O_4@SnO_2:Er^{3+},Yb^{3+}–APTES nanocarrier for microwave-triggered controllable drug release, and study of the loading and release mechanisms using microcalorimetry

Hongxia Peng[1,2], Bin Cui*[1], Weiwei Zhao[1], Xiaotong Zhao[1], Yingsai Wang[1], Zhuguo Chang[1], Yaoyu Wang[1]

Author family names: Peng, Cui, Zhao, Zhao, Wang, Chang, and Wang

1 Key Laboratory of Synthetic and Natural Functional Molecule Chemistry (Ministry of Education), Shaanxi Key Laboratory of Physico-Inorganic Chemistry, School of Chemistry & Materials Science, Northwest University, 229 North Taibai Avenue, Xi'an 710069, P.R. China

2 Department of Chemistry & Materials Science, Hunan University of Humanities, Science and Technology, Lou'di 137400, P.R. China

* Corresponding author. Tel.: +86-029-81535030; Fax: +86-029-81535021.

E-mail address: cuibin@nwu.edu.cn.

New Journal of Chemistry Accepted Manuscript

Abstract

We fabricated an efficient microwave-triggered controlled-release nanocarrier system using Fe_3O_4@SnO_2:Er^{3+},Yb^{3+}–APTES multifunctional core–shell nanoparticles. We also studied the drug loading and release mechanisms by means of microcalorimetry. The thermodynamic parameter values for loading (ΔH = –42.64 kJ mol^{-1}, ΔS = –452.98 J mol^{-1} K^{-1}) showed that the main interaction between the nanocarrier and drug molecules is relatively weak hydrogen bonding. The molar enthalpy (ΔH) of the drug-release process was 10.30 kJ mol^{-1}, which indicates an endothermic process. This suggests that drug release can be controlled by microwave heating. When energy provided from the medium rises above the hydrogen bond energy, the hydrogen bond breaks and the nanocarrier begins to release the drug. The release profile can be controlled by the duration and number of cycles of microwave application. Approximately 71% of ibuprofen was released after four cycles. The microwave-stimulated, thermally sensitive, multifunctional nanoparticles therefore represent a new system with potential utility for on-command drug release, and the fluorescence properties allow *in situ* monitoring.

Key words: Fe_3O_4@SnO_2:Er^{3+},Yb^{3+}; Magnetic; Up-conversion luminescence; Microwave-stimulated release; Controlled drug release; Microcalorimetry

1. Introduction

Multifunctional nanocarriers that combine several useful properties in a single nanostructure have become one of the dominant areas of research in drug-delivery systems[1,2]. Nanocarriers with multifunctional components can interact with an external magnetic field positioned near a specified area that is targeted for drug delivery and fluorescence imaging, and the release process can be monitored and tracked based on changes in the luminescence intensity[3-5]. In addition, drug release

New Journal of Chemistry Accepted Manuscript

can be triggered through the application of an external stimulus. For example, some recently developed delivery systems have been triggered by means of ultrasound, light, pH changes, redox conditions, temperature, and magnetic fields, thereby minimizing the systemic side-effects (i.e., off-target effects) of the drugs[6-8].

For medical applications, an external and noninvasive method of actuation is preferable to better control the therapeutic effects. Thus, temperature-stimulated drug release has generated increasing interest because of the high selectivity, easily controllable modulation, and noninvasive character of this approach[9,10]. Several temperature-responsive nanocarriers have been designed based on heating induced by light or alternating magnetic fields, which lead to excitation of the nanocarrier and liberation of the drug molecules. Thomas et al.[11] synthesized magnetic Zn-Fe_3O_4@SiO_2 nanocomposites, and found that the application of an alternating magnetic field generated localized internal heating, causing disassembly of the molecular machines and release of the attached drugs. Gui et al.[12] developed a photosensitive liposome that contained Au nanoparticles and doxorubicin embedded in the liposome's internal aqueous cavity, and used this structure as a liposome-based drug nanocarrier. However, the use of light and alternating magnetic fields to induce local heating may cause overheating and damage to the surrounding tissues as a result of surface heating, a slow heating rate, shallow tissue penetration, and difficulty controlling the temperature[13-17]. Fortunately, the lack of an effective, external control for *in vivo* applications can be overcome by taking advantage of a new class of multifunctional materials that are capable of absorbing microwaves.

Materials capable of absorbing microwaves and undergoing heating when irradiated by a microwave source can be employed as a non-invasive local heat source [18]. Microwave irradiation provides better thermal efficiency, high tissue penetration

New Journal of Chemistry Accepted Manuscript

depth (10 to 15 cm), and accurate control by varying parameters such as the power and duration of the irradiation[19]. Research has revealed that $SnO_2:Er^{3+},Yb^{3+}$ nanoparticles can rapidly absorb microwaves and efficiently convert the microwave energy into localized heat, thereby producing a selective and sensitive microwave-induced thermal effect[20]. In addition, $SnO_2:Er^{3+},Yb^{3+}$ nanoparticles are easy to fabricate, inexpensive, and exhibit up-conversion luminescence that would support monitoring of the *in situ* drug release [21]. Fe_3O_4 has strong magnetic properties, and has been widely used in drug delivery, cell separation, and magnetic-resonance imaging. Fe_3O_4 and $SnO_2:Er^{3+},Yb^{3+}$ demonstrate lower toxicity and better biocompatibility low toxicity and high biocompatibility based on *in vivo* cytotoxicity evaluations[22]. As a result, nanoparticles that combine these two materials can be employed as drug-delivery nanocarriers and as non-invasive local heat sources.

For a delivery system to be effective, favorable interactions between the drug and the nanocarrier (i.e., an appropriate bond type and strength) are essential[23]. Microcalorimetry is a sensitive technique for studying the enthalpy of interactions between molecules in a solution. This approach can accurately monitor and record the thermal changes during an interaction process, and can provide information on the thermodynamics and molecular dynamics of the system[24]. Wang and Han[23] studied the interactions of hydrophobically modified poly(acrylamide) and unmodified poly(acrylamide) with sodium dodecyl sulfate or tetradecyltrimethyl-ammonium bromide by means of flow microcalorimetry. However, this method has not been used for drug delivery systems.

In the present study, we combined the advantages of $SnO_2:Er^{3+},Yb^{3+}$ nanoparticles with those of Fe_3O_4 and 3-aminopropyltriethoxysilane (APTES) to create a new drug delivery system that responds to microwave irradiation (Scheme 1).

New Journal of Chemistry Accepted Manuscript

This novel approach to drug delivery allows loading of the drug on the surface of the nanoparticles by means of hydrogen bonding, with stable retention of the drug on the nanocarrier surface at normal body temperatures, and controlled release of the drug upon local heating generated by conversion of microwaves into heat by the Fe_3O_4@SnO_2:Er^{3+},Yb^{3+} nanoparticles. The particles also exhibit good magnetization and up-conversion luminescence properties, which will allow simultaneous targeting and monitoring of the loaded drug. We chose ibuprofen as a model drug to evaluate the loading and release function of the nanocarrier, and studied the loading and release mechanisms by means of microcalorimetry. This provided a simple method to monitor the interactions between the nanocarrier and the drug.

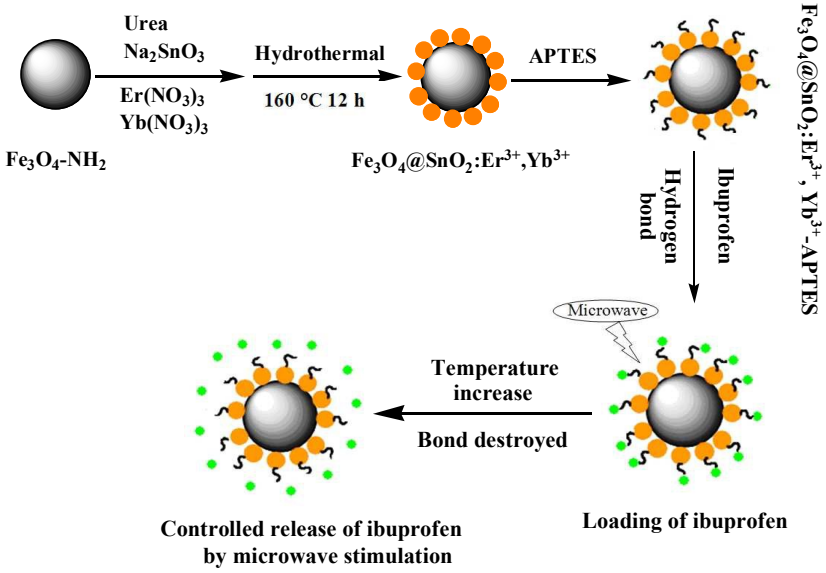

Scheme 1. Illustration of the process of creating Fe_3O_4@SnO_2:Er^{3+},Yb^{3+}–APTES nanoparticles and the controlled release of a loaded drug (ibuprofen) by microwave stimulation.

2. Experimental section

2.1 Materials and Characterization

All the chemical reagents used in this experiment were of analytical grade and were used without further purification. Ferric chloride hexahydrate ($FeCl_3 \cdot 6H_2O$,

New Journal of Chemistry Accepted Manuscript

purity 99%), sodium acetate (CH_3COONa, purity ≥99.0%), ethylenediamine ($C_2H_8N_2$, purity ≥98.0%), and 3-aminopropyltriethoxysilane ($C_9H_{23}NO_3Si$, APTES, purity 99%) were purchased from the Shanghai Chemical Reagent Factory (Shanghai, China). Ibuprofen was purchased from the Jiangsu Hengrui Medicine Factory (Lianyungang, China). Sodium nitrate (Na_2SnO_3, purity 99%) and carbamide ($CO(NH_2)_2$) were purchased from the National Reagent Corporation (Shanghai, China). 3-(4,5-dimethyl-thiazol-2-yl)-2,5-diphenyltetrazolium bromide (MTT) was purchased from the Sigma Chemical Company. A human breast cancer cell line (MCF-7) was purchased from the Key GEN Biotechnology Company (Nanjing, China). Deionized water was used in all of the experiments.

X-ray diffraction (XRD) patterns of the samples were measured using an AXS D8 Advance Diffractometer (Bruker, Bremen, Germany) with Cu K_α radiation (λ = 0.15406 nm) at 40 kV and 40 mA. The morphologies and structures of the as-prepared samples were inspected using a JEM 2010 transmission electron microscope (JEOL, Peabody, MA). Room-temperature Fourier-transform infrared (FT-IR) spectra of the samples, mounted on KBr discs, were recorded using a PerkinElmer (Waltham, MA, USA) 100 S spectrometer. Ultraviolet–visible light (UV–vis) spectral adsorption values were measured using a UV-1800 spectrophotometer (Shimadzu, Kyoto, Japan). The up-conversion emission spectra of the samples were recorded with a Hitachi (Tokyo, Japan) F-4500 fluorescence spectrometer. An adjustable laser diode (980 nm, 2 W) was used as the excitation source. Magnetization measurements were performed at 300 K using an MPMS-XL-7 superconducting quantum interference device (SQUID) magnetometer.

Drug release under microwave stimulation was controlled using an HBS-C medical microwave apparatus (Human Biosystems Inc., Palo Alto, CA, USA), at a

New Journal of Chemistry Accepted Manuscript

working frequency of 2450±30 MHz and a microwave power of 0 to 150 W. The thermodynamics of the drug loading and release system were measured using an RD496-2000 Calvet microcalorimeter (Mianyang CAEP Thermal Analysis Instrument Company, Mianyang, China). The microcalorimeter was calibrated using the Joule effect, and its sensitivity was 64.28±0.04 uV mW^{-1} at 298.15 K. Absorbance of MTT by treated cells in the MTT assay was measured using an RT-6000 microplate reader (Rayto Life and Analytical Sciences Co. Ltd., Shenzhen, China). The electromagnetic parameters of the Fe_3O_4@SnO_2:Er^{3+},Yb^{3+} nanoparticles were measured using a N5230A vector network analyzer (Agilent Technologies, Santa Clara, CA, USA) with the transmission and reflection mode in the 2 to 18 GHz band. All the measurements were performed at room temperature.

2.2 Synthesis and modification of the Fe_3O_4@SnO_2:Er^{3+},Yb^{3+} nanoparticles

Amino-functional magnetic Fe_3O_4 nanoparticles were prepared by the solvothermal method[33]. SnO_2:Er^{3+},Yb^{3+} was layered on the surface of the magnetic Fe_3O_4 nanoparticles using a hydrothermal method. In a typical procedure, 0.1 g of as-prepared Fe_3O_4 nanoparticles were dispersed in 15 mL of ethanol and 25 mL of H_2O. The mixture was sonicated for 5 min followed by the addition of 1.2 g of carbamide and 0.2 g of Na_2SnO_3, and aqueous solutions of $Er(NO_3)_3$ (5 mL, 0.02 mol L^{-1}) and $Yb(NO_3)_3$ (5 mL, 0.1 mol L^{-1}) were added with constant stirring for 30 min. The solution was then transferred into a Teflon-lined stainless-steel autoclave (50 mL capacity). The autoclave was then heated to 433.15 K and maintained at that temperature for 12 h, and then allowed to cool to room temperature. The resultant products were separated using a magnet, thoroughly washed with ethanol and deionized water several times, and further dried at 333.15 K overnight.

New Journal of Chemistry Accepted Manuscript

Next, 0.1 g of Fe_3O_4@SnO_2:Er^{3+},Yb^{3+} nanoparticles were dispersed in 4.0 mL of ethanol and 40 mL of H_2O. The solution was stirred for about 10 min at room temperature, then 2.5 mL APTES was added and the solution was heated to 353.15 K under vigorous mechanical stirring. After 3 h, the product was precipitated by centrifuging for 10 min at 8000×*g*, then washed with ethanol and de-ionized water and dried at 333.15 K overnight. The resulting products were the Fe_3O_4@SnO_2:Er^{3+},Yb^{3+}–APTES nanoparticles.

2.3 Drug loading and controlled release

To monitor the process of drug loading, 1 mL of the solution was withdrawn at predetermined time intervals and immediately replaced by an equal volume of sodium chloride solution to keep the volume constant. The withdrawn solution was diluted in 1 mL of deionized water and the ibuprofen content was determined based on absorption at 220 nm using the UV–vis spectrophotometer. Over time, the intensity of the absorption band at 220 nm slowly decreased, suggesting that the amount of ibuprofen released into the solution increased. Until the loading is close to balance, the free ibuprofen weight in the solution was determined by means of UV–vis spectrophotometry using the Lambert–Beer law, with the concentration of ibuprofen (*C*) calculated according to an obtained standard absorption curve for ibuprofen ($C = 0.0903A + 0.0013$, $r = 0.9983$). The amount of the drug loaded was calculated based on the free ibuprofen in the solution. Drug loading (w/w %) = M_{ads}/M_{add}, where M_{ads} is the mass of drug adsorbed, and M_{add} is the mass of drug added during the loading process.

The amount of ibuprofen released during four microwave irradiation cycles was evaluated to study the ability to control triggering and release of the drug. To do so, 2 mL of Fe_3O_4@SnO_2:Er^{3+},Yb^{3+}–APTES–ibuprofen (0.1 mg mL^{-1}) in physiological

New Journal of Chemistry Accepted Manuscript

saline solution was irradiated with microwaves for four on/off cycles. For each cycle, the sample was first irradiated for 6 min at 8 W and then cooled to room temperature (298.15 K) for 60 min before measuring the UV-vis intensity of the sample.

2.4 Thermodynamics of the drug loading and release systems

The thermodynamic characteristics of the drug loading process were monitored using an RD496-2000 microcalorimeter at 309.65 K. The calorimetric constant at 309.65±0.01 K was determined by the Joule effect before the experiment; this equaled 64.25±0.050 $\mu V \cdot mW^{-1}$. The enthalpy (*H*) of a solution of KCl in deionized water was measured and found to be 17.585±0.045 $kJ \cdot mol^{-1}$, which is in good agreement with the value of 17.581±0.039 $kJ \cdot mol^{-1}$ reported by Can et al.[40]; the deviation of the experimental result from the latter value is 0.03%, which indicates that the calorimetric system was accurate and reliable. We dissolved 2.5 mg of ibuprofen and 2.5 mg of the nanocarrier (Fe_3O_4@SnO_2:Er^{3+},Yb^{3+}–APTES) in 1.50 mL of dimethyl sulfoxide (DMSO) to load the drug at 309.65 K under atmospheric pressure. We chose DMSO as the solvent because it is a good solvent for ibuprofen and has little or no effect on the drug's pharmacological action. The calorimetry curves described the entire drug loading process. The obtained product was denoted as Fe_3O_4@SnO_2:Er^{3+},Yb^{3+}–APTES–ibuprofen.

The thermodynamic characteristics of the drug release process were measured using the same microcalorimeter. To do so, we dissolved 4.4 mg of the prepared sample of in 1.50 mL of sodium chloride solution (similar to the concentration of normal saline for human blood, at pH 5.8) with gentle stirring while sealed in a membrane mixing vessel (volume: 8.5 mL) at 323.15 K under atmospheric pressure. The calorimetric curves described the entire drug release process.

New Journal of Chemistry Accepted Manuscript

2.5 MTT assays

To evaluate the cytotoxicity of the nanocarrier and the microwave-thermal effect after microwave irradiation, we performed an MTT assay using MCF-7 cells, which are commonly used as a representative cancer cell line[14]. The MCF-7 cells were cultured in 96-well microtiter plates and incubated at 310.15 K in 5% CO_2 for 24 h. The cells were incubated in a culture medium containing Fe_3O_4@SnO_2:Er^{3+},Yb^{3+}-APTES at 0.1 or 0.2 mg mL^{-1} for three durations (6, 12, or 24 h), respectively. Next, 150 μL of MTT solution (0.5 mg mL^{-1}) was added to each well. After 4 h, the remaining solution was removed, and 150 μL of DMSO was added to each well to dissolve the formazan crystals. The absorbance was measured at 490 nm with the RT-6000 microplate reader. The cells were then irradiated with microwaves at 8 W for different times. Each irradiation lasted for 10 min, followed by a 2 h interval before the next irradiation. After irradiation, the cells were incubated at 310.15 K for 24 h. We expressed the cell viability as the ratio of absorbance by the treated cells (incubated with the nanoparticles or irradiated with microwaves) to that of the untreated cells.

3. Results and Discussion

3.1 Morphology and structural composition

Fig. 1 shows the XRD patterns for the Fe_3O_4, SnO_2:Er^{3+},Yb^{3+}, and Fe_3O_4@SnO_2:Er^{3+},Yb^{3+} nanoparticles. Fig. 1a shows that the magnetite cores were well indexed to the cubic spinel structure of Fe_3O_4 (JCPDS card no. 65-3107) with lattice constant a=b=c= 8.39 Å. Fig. 1b shows a rutile structure as all the diffraction peaks could be indexed as per the JCPDS card no.41-1445 corresponding to Bragg diffractions of the rutile structured SnO_2 with tetragonal lattice constant a=4.74Å and c=3.19 Å. For the Fe_3O_4@SnO_2:Er^{3+},Yb^{3+} nanoparticles (Fig. 1c), peaks of magnetite with a cubic spinel structure

New Journal of Chemistry Accepted Manuscript

were observed, revealing that the Fe_3O_4 nanoparticles did not change their phases. The additional diffraction peaks at 26.64°, 34.00°, 51.78°, 65.43°, and 78.84° can be readily indexed to the rutile-type SnO_2 nanostructure, which suggested successful crystallization of SnO_2:Er^{3+},Yb^{3+} on the surface of the Fe_3O_4 nanoparticles. In addition, we detected no peaks of other phases, indicating that indicating that substitutional doping of Er^{3+} and Yb^{3+} ions with higher ionic radii in the SnO_2 host lattice rather than located at the surface of SnO_2 particles[20].

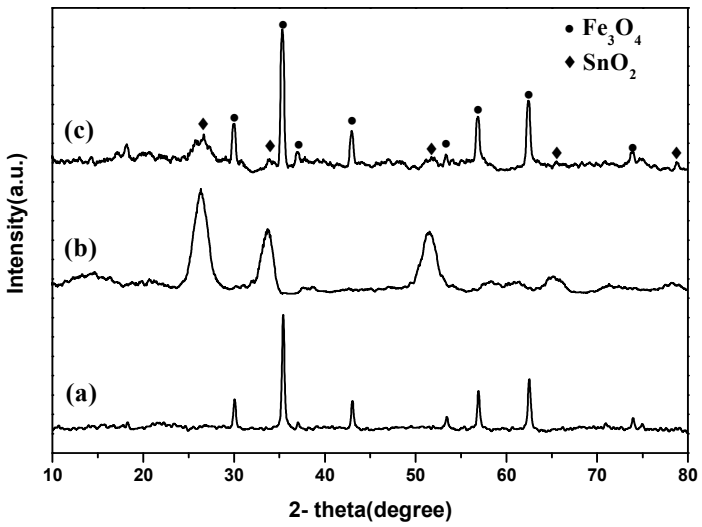

Fig. 1 XRD patterns of the samples: (a) Fe_3O_4, (b) SnO_2:Er^{3+},Yb^{3+}, and (c) Fe_3O_4@SnO_2:Er^{3+},Yb^{3+}.

We used an easy hydrothermal method to prepare luminescent SnO_2:Er^{3+},Yb^{3+} nanoparticles layered on the surface of the Fe_3O_4 nanoparticles. The surface amino group of the Fe_3O_4 nanoparticles bonded with the metal ions via an N–Sn^{4+} coordination bond. Fig. 2 shows that the average diameter of the Fe_3O_4@SnO_2: Er^{3+},Yb^{3+} nanoparticles was about 50 nm and the diameter of the SnO_2:Er^{3+},Yb^{3+} particles was about 3 nm. Moreover, the obvious lattice fringes in the high-resolution TEM image (Fig. 2c) confirm the successful crystallization of SnO_2:Er^{3+},Yb^{3+} on the surface of Fe_3O_4, which is in good agreement with the wide-angle XRD results (Fig. 1). The spacing in the shell region was about 0.3325 and 0.2633 nm, respectively, for

New Journal of Chemistry Accepted Manuscript

the (110) plane and the (101) plane of SnO_2, versus about 0.2518 nm in the core region, corresponding to the (311) plane of Fe_3O_4. The surface modification by APTES brought free amino groups to the surface, offering an opportunity for Fe_3O_4@SnO_2:Er^{3+},Yb^{3+} to be used as a nanocarrier for drugs capable of bonding to these groups.

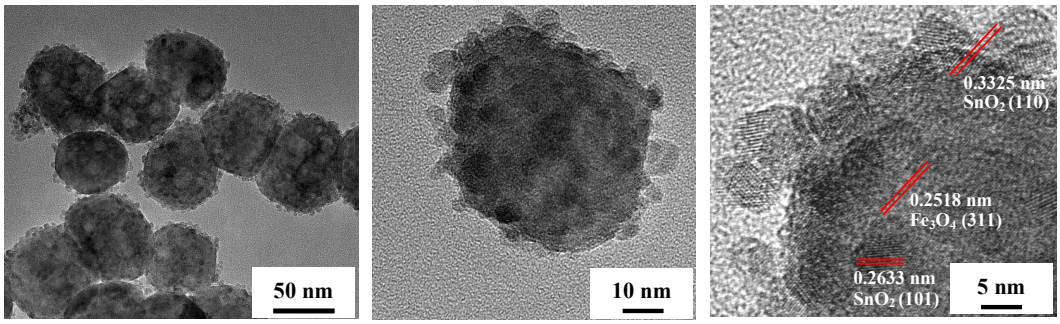

Fig. 2 Images of the samples: (a and b) TEM and (c) HRTEM images of Fe_3O_4@SnO_2:Er^{3+},Yb^{3+}

Fig. 3 shows the FT-IR spectra of Fe_3O_4@SnO_2:Er^{3+},Yb^{3+}–APTES, Fe_3O_4@SnO_2:Er^{3+},Yb^{3+}–APTES–ibuprofen, and pure ibuprofen. There was strong absorption at 495 cm^{-1}, which can be assigned to the Sn-O stretching vibration[24]. Similarly, the presence of adsorbed water molecules is revealed by the band for ν (H_2O) at 3430 cm^{-1}[25]. Fig. 3a focuses on the changes caused by modification with APTES. The additional absorption bands between 900 and 1300 cm^{-1} can be assigned to vibrations involving Si atoms in the siloxanes and in the non-condensed organosilane groups[26]. The band at 1050 cm^{-1} is assigned to Si-O-Si, and that at 1190 cm^{-1} is assigned to Si-O-C[27]. The band at 1190 cm^{-1} could also be due to Sn-O-Si groups, which would indicate a covalent interaction[28]. However, we hypothesize that both Si-O-C and Sn-O-Si vibrations are involved in this absorption. An absorption band centered at 1597 cm^{-1} can be assigned to the δ N-H stretching vibration in NH_2[29], which confirms the presence of reactive NH_2 groups introduced at the surface of the Fe_3O_4@SnO_2:Er^{3+},Yb^{3+} nanoparticles. The FT-IR spectrum of

New Journal of Chemistry Accepted Manuscript

Fe_3O_4@SnO_2:Er^{3+},Yb^{3+}–APTES–ibuprofen (Fig. 3b) shows a strong peak at 1413 cm^{-1}, which corresponds to the characteristic stretching vibrations of C=C in the backbone of the aromatic phenyl ring [30]. The characteristic alkyl (C-H) vibrations at 2930 cm^{-1} and a band that can be assigned to C=O (1765 cm^{-1}) are apparent, but show a slight decrease in absorption compared with the corresponding positions for pure ibuprofen (Fig. 3c) [30], which confirms the successful incorporation of ibuprofen at the surface of the Fe_3O_4@SnO_2:Er^{3+},Yb^{3+}–APTES nanoparticles. We detected no additional peaks for new chemical bonds, which indicated that no chemical reaction occurred between Fe_3O_4@SnO_2:Er^{3+},Yb^{3+}–APTES and ibuprofen. The ibuprofen molecules therefore appear to have been incorporated on the surface of the nanoparticles through non-covalent bonds.

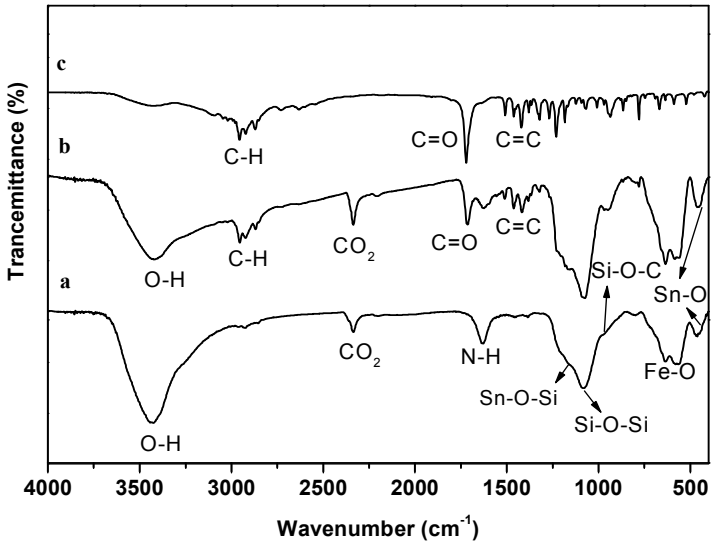

Fig. 3. The FT-IR spectra of (a) Fe_3O_4@SnO_2:Er^{3+},Yb^{3+}–APTES, (b) Fe_3O_4@SnO_2:Er^{3+},Yb^{3+}–APTES–ibuprofen and (c) pure ibuprofen.

3.2 Up-conversion luminescence and magnetic properties

To investigate the up-conversion luminescence properties of the nanoparticles, we recorded these spectra at room temperature. Fig. 4A shows that the green emission band centered at 545 nm can be attributed to the $^4S_{3/2} \rightarrow {}^4I_{15/2}$ electron transition of the

New Journal of Chemistry Accepted Manuscript

Er^{3+} ions[20]. The red emission at 660 nm can be ascribed to the $^4F_{9/2} \rightarrow {}^4I_{15/2}$ transition of the Er^{3+} ions[20]. Here, Yb^{3+} functions as a sensitizer. The sensitization by the Yb^{3+} ions can significantly improve the conversion efficiency of the Er^{3+} ions. This is because Yb^{3+} ions have a large absorption cross-section near a wavelength of 980 nm, and they can transfer the excitation energy to the nearby Er^{3+} ions through resonance [20]. The decreased up-conversion emission of the $Fe_3O_4@SnO_2:Er^{3+},Yb^{3+}$–APTES (Fig. 4b) and $Fe_3O_4@SnO_2:Er^{3+},Yb^{3+}$–APTES–ibuprofen (Fig. 4c) nanoparticles could be caused by the reactive introduced amino groups and the drug at their surface, leading to energy loss at the surface and fluorescence quenching by the introduced organic groups[34]. Although the up-conversion luminescence intensity of the $Fe_3O_4@SnO_2:Er^{3+},Yb^{3+}$–APTES and $Fe_3O_4@SnO_2:Er^{3+},Yb^{3+}$–APTES–ibuprofen nanoparticles decreased, the intensity was still strong enough to permit bio-imaging.

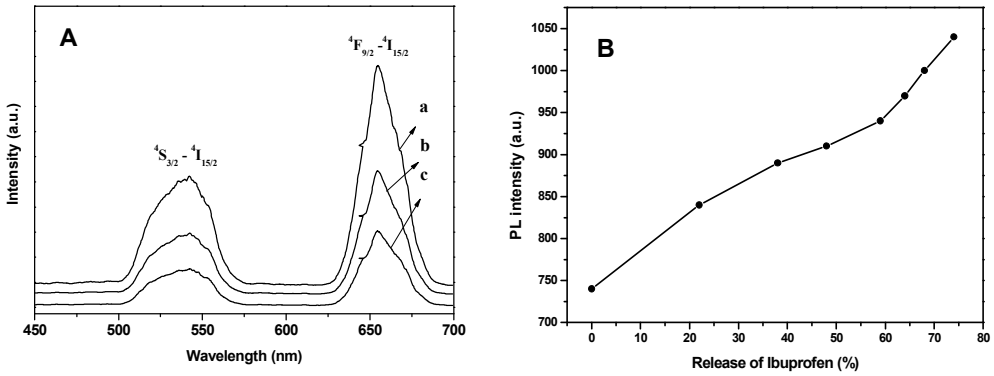

Fig. 4A Up-conversion emission spectra (λ_{ex} = 980 nm) of (a) $Fe_3O_4@SnO_2:Er^{3+},Yb^{3+}$, (b) $Fe_3O_4@SnO_2:Er^{3+},Yb^{3+}$–APTES, and (c) $Fe_3O_4@SnO_2:Er^{3+},Yb^{3+}$–APTES–ibuprofen.

Fig. 4B Photoluminescence emission intensity of $Fe_3O_4@SnO_2:Er^{3+},Yb^{3+}$–APTES–ibuprofen as a function of cumulative released ibuprofen

Moreover, here it is of great interest and importance to note the relationship between the up-conversion luminescence emission intensity of $Fe_3O_4@SnO_2:Er^{3+},Yb^{3+}$–APTES–ibuprofen system and the cumulative released amount of ibuprofen (Fig. 4B). The up-conversion luminescence intensity increases

New Journal of Chemistry Accepted Manuscript

with the cumulative released drug until ibuprofen is completely released. This may be related with the quenching effect of $SnO_2:Er^{3+},Yb^{3+}$ emission caused by the organic groups with high vibration frequencies in NH_2 and $SnO_2:Er^{3+},Yb^{3+}$ molecules [38]. The quenching effect is weakened with the drug release amount, resulting in the enhancement of up-conversion luminescence intensity. This correlation between the up-conversion luminescence intensity and drug release extent can be potentially used as a probe for monitoring the drug release and efficiency. These results also suggest that the magnetic and fluorescence properties of the nanocomposites can be modified in different ways by the addition of different drugs or organic molecules, thereby permitting the design of new materials and microstructures.

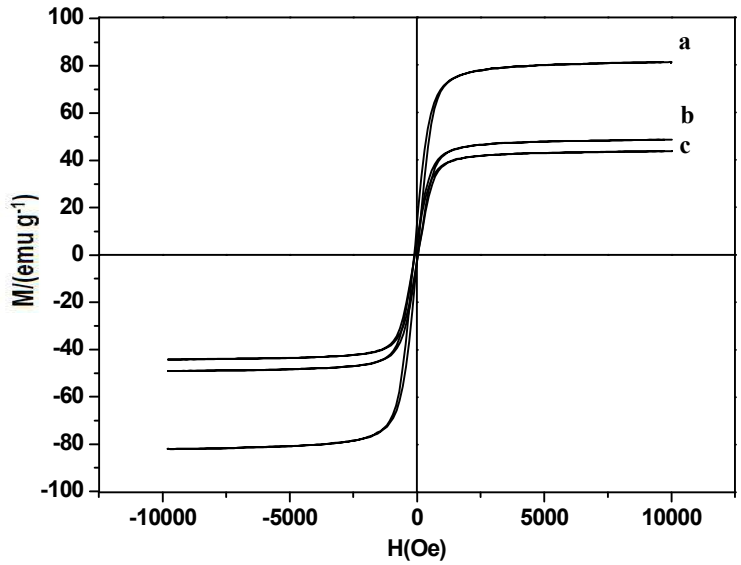

Fig. 5. Hysteresis loops for (a) Fe_3O_4, (b) $Fe_3O_4@SnO_2:Er^{3+},Yb^{3+}$, and (c) $Fe_3O_4@SnO_2:Er^{3+},Yb^{3+}$–APTES–ibuprofen.

The magnetic properties of the nanoparticles were characterized using a SQUID magnetometer at 300 K. Magnetic measurements showed that Fe_3O_4, $Fe_3O_4@SnO_2:Er^{3+},Yb^{3+}$, and $Fe_3O_4@SnO_2:Er^{3+},Yb^{3+}$–APTES–ibuprofen had magnetization saturation values of 85.92, 48.37, and 42.00 emu g^{-1}, respectively (Fig. 5). It is noteworthy that the $Fe_3O_4@SnO_2:Er^{3+},Yb^{3+}$ and $Fe_3O_4@SnO_2:Er^{3+},Yb^{3+}$

New Journal of Chemistry Accepted Manuscript

–APTES–ibuprofen retained strong magnetization, indicating their suitability for magnetic targeting and separation as a drug nanocarrier. The saturation magnetization of the Fe_3O_4@SnO_2:Er^{3+},Yb^{3+} and Fe_3O_4@SnO_2:Er^{3+},Yb^{3+}–APTES–ibuprofen nanoparticles occurred at smaller values than for the Fe_3O_4 nanoparticles. This is likely due to the decreased proportion of Fe_3O_4 in the nanoparticles that results from the addition of a non-magnetic shell [35,36]. The Fe_3O_4@SnO_2:Er^{3+},Yb^{3+}–APTES–ibuprofen nanoparticles still possess excellent magnetic responsivity and redispersibility, which is important in terms of their practical manipulation[34].

3.3 Microwave absorption

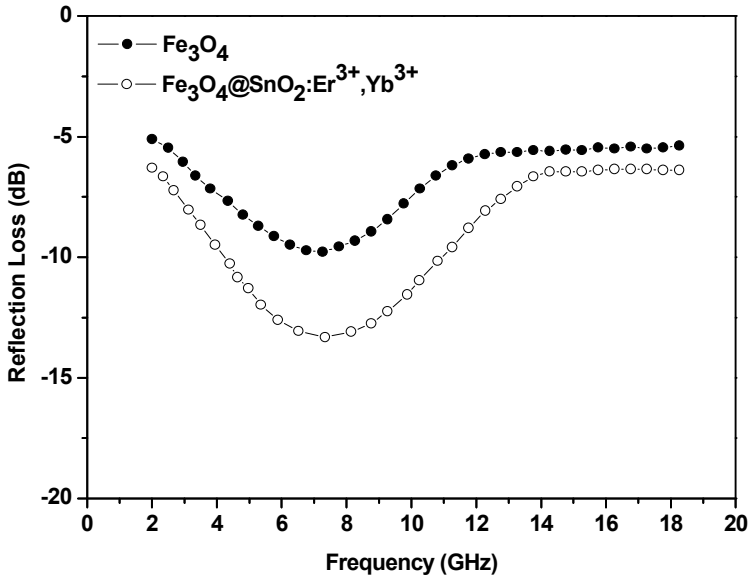

Fig. 6. Microwave reflection loss curves for (a) Fe_3O_4 and (b) Fe_3O_4@SnO_2:Er^{3+},Yb^{3+} at a thickness of 2 mm.

To further study the microwave absorption properties, we calculated the reflection loss using the equations for transmission-line theory [37]. Fig. 6 shows that at a thickness of 2 mm, the maximum reflection loss of the Fe_3O_4 particles is −9.79 dB at 7 GHz; in contrast, the Fe_3O_4@SnO_2:Er^{3+},Yb^{3+} nanoparticles show their maximum reflection loss of -13.35 dB at about 7.5 GHz. The incorporation of the dielectric SnO_2:Er^{3+},Yb^{3+} into the Fe_3O_4-based microwave absorber may generate a high

New Journal of Chemistry Accepted Manuscript

dielectric constant and reflection loss due to an effective interface between the dielectric and magnetic materials. Therefore, the interfacial polarization and the associated relaxation will contribute to enhanced microwave absorption. The thickness of the material has a great impact on the microwave absorption properties; increasing the thickness leads to lower microwave absorption frequencies[29]. The results suggest that the Fe_3O_4@SnO_2:Er^{3+},Yb^{3+} nanoparticles have excellent microwave absorption properties.

3.4 Drug loading of the Fe_3O_4@SnO_2:Er^{3+},Yb^{3+}–APTES drug delivery system

To allow loading and release of drugs by means of microwave irradiation, APTES was added to the particle surface to introduce reactive amino groups. Ibuprofen was selected as a model drug, as it has been extensively investigated for sustained and controlled drug delivery due to its short biological half-life (2 h) and good pharmacological activity. To properly understand the loading process, we must first understand the molecular structure of ibuprofen, which is an aromatic compound that contains a carboxylic acid functional group (Scheme 2). We selected APTES because it can promote the formation of hydrogen bonds between ibuprofen and Fe_3O_4@SnO_2:Er^{3+},Yb^{3+}–APTES. The hydrogen bonds remain stable at physiological temperatures, but break when heated. Therefore, this synthetic approach has the potential to allow easy control of drug molecule delivery by means of local heating.

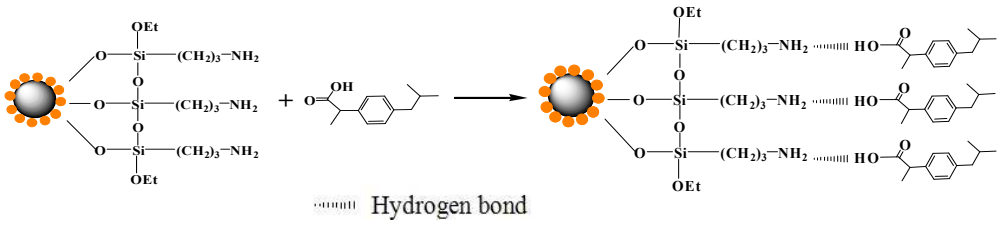

Scheme 2. Schematic representation of the loading of ibuprofen onto the Fe_3O_4@SnO_2:Er^{3+},Yb^{3+}–APTES nanoparticles.

New Journal of Chemistry Accepted Manuscript

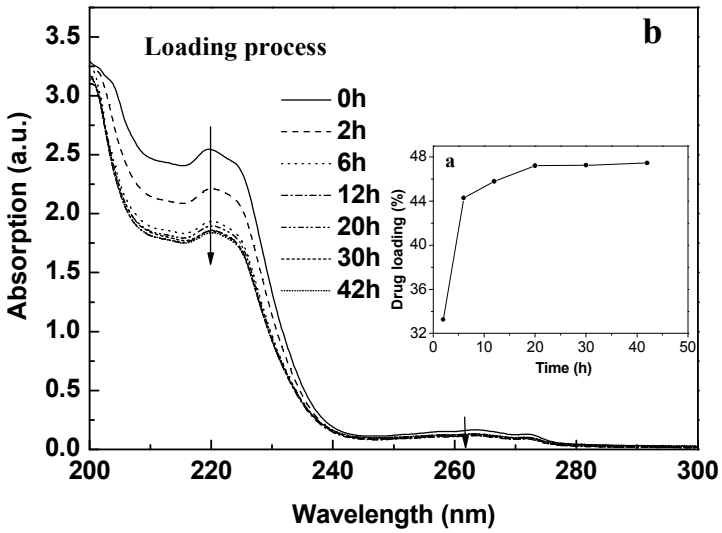

Fig. 7. Kinetics analysis of drug loading: (a) drug loading versus time and (b) the corresponding UV–vis spectra.

Fig. 7 shows the drug loading process as a function of time at room temperature and pH = 7 in deionized water. During the initial stage, the loading rate reaches 33% within 2 h. With increasing time, the intensity of the absorption band at 220 nm decreased, suggesting an increase in the ibuprofen load. The UV-vis spectra showed no change in the absorption peak (220 nm) after 20 h of loading. We found that approximately 47% of the total ibuprofen was loaded onto the surface of the Fe_3O_4@SnO_2:Er^{3+},Yb^{3+}–APTES nanoparticles by around 20 h. These results indicate that the nanoparticles have a good drug loading capacity, but that the loading occurs relatively slowly.

We dissolved 2.5 mg of ibuprofen and 2.5 mg of the Fe_3O_4@SnO_2:Er^{3+},Yb^{3+}–APTES nanoparticles in 1.50 mL of DMSO to load the drug at 309.65 K under atmospheric pressure. Fig. 8 shows the curves that describe the entire drug loading process. The heat energy ($-Q$) can be calculated through integration of the thermogram curve (Fig. 8a) and the change in molar enthalpy (ΔH)

New Journal of Chemistry Accepted Manuscript

can be calculated from the equation $\Delta H = \frac{-Q}{n}$, Table 1 summarizes the thermodynamic results.

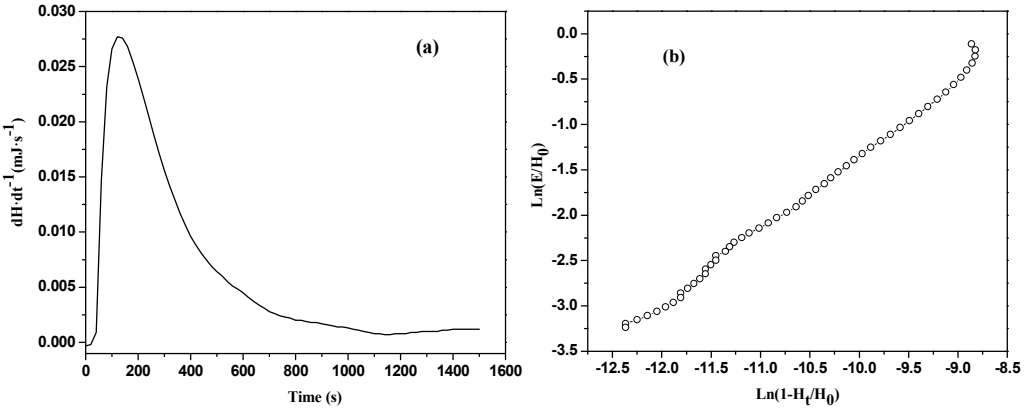

Fig. 8 (a) The exothermic curve for the drug loading process; (b) The linear relationship of $\ln[1-(\frac{H_t}{H_0})]$ and $\ln[\frac{1}{H_0}(\frac{dH}{dt})]$.

Based on our experimental data and these calculated thermodynamic parameters, the kinetic parameters of the drug-loading processes were obtained through Eq. 6, which was deduced from equations 1–5 [35]:

$$\Delta G_{\neq} = -RT\ln k^{\neq} \quad (1)$$

$$k = \frac{RT}{Nh}k^{\neq} \quad (2)$$

Then

$$\Delta G_{\neq}^{\theta} = RT\ln[\frac{RT}{Nhk}] \quad (3)$$

$$k = \frac{RT}{Nh}e^{-\Delta G_{\neq}^{\theta}/RT} = \frac{RT}{Nh}e^{(T\Delta S_{\neq}^{\theta}-\Delta H_{\neq}^{\theta})/RT} = \frac{RT}{Nh}e^{\Delta S_{\neq}^{\theta}/R}e^{-\Delta H_{\neq}^{\theta}/RT} \quad (4)$$

From these equations, we can obtain:

$$\ln\frac{k}{T} = (\frac{\Delta S_m^{\theta}}{R} + \ln\frac{k_B}{h}) - \frac{\Delta H_m^{\theta}}{RT} \quad (5)$$

Eq.5 can be expressed as follows:

$$\ln\frac{k}{k_B T} = \frac{\Delta S}{R} - \frac{\Delta H}{RT} \quad (6)$$

New Journal of Chemistry Accepted Manuscript

Substituting $k = 10^{-3.66}\ s^{-1}$, $k_B = 1.38\times10^{-23}$ J K^{-1}, $h = 6.626\times10^{-23}$ J s^{-1}, and the ΔH values from Table 1, and $T = 309.65$ K into Eq. 6, ΔS can be obtained. ΔG can then be obtained by inputting ΔH and ΔS into the following formula:

$$\Delta G = \Delta H - T \cdot \Delta S \quad (7)$$

From the calculated values in Table 1, we can see that during the whole drug-loading process, $\Delta H < 0$. That is, the bonding between the drug molecules and the nanocarrier is an exothermic reaction. We know that the main reaction force can be determined for different chemical systems according to the thermodynamic parameters at different temperatures. (The bond energy for hydrogen-bond interactions is about 200 kJ mol^{-1}, generally for 5 to 30 kJ mol^{-1}; the van der Waals force is commonly 0.4 to 4.0 kJ mol^{-1}.) According to the thermodynamic parameters, the main force acting between the nanocarrier and ibuprofen can be determined. In this context, Ross and Subramanian [36] reported that when $\Delta H < 0$ (or $\Delta H \approx 0$) and $\Delta S > 0$, electrostatic forces dominate the interaction; when $\Delta H < 0$ and $\Delta S < 0$, van der Waals interactions or hydrogen bonds dominate the interaction; and when $\Delta H > 0$ and $\Delta S > 0$, hydrophobic interactions dominate the interaction.

By applying this analysis to the drug-loading system, it appears that van der Waals forces or hydrogen bonds were the most important factor contributing to the observed ΔH and ΔS (Table 1) and hence to the stability of the drug-loading process. The thermodynamic parameters are too large for van der Waals forces, thus the bonding must be via hydrogen bonds. Hydrogen bonds are weak, and are therefore easy to break. The negative value of the entropy of activation (ΔS) indicates that the drug-loading process in DMSO produces a more ordered system.

In the drug loading process, the Gibbs free energy change (ΔG) in Table 1 is an important parameter, as it reflects the binding degree and stability of the formed

New Journal of Chemistry Accepted Manuscript

adduct. ΔG was positive, indicating that the drug-loading process in DMSO is stable at 309.65 K. In other words, this is a thermodynamically stable system for the drug-loading process in DMSO.

Table 1. Thermodynamic parameters for the interaction forces between the nanocarrier nanoparticles and the drug.

Sample mass (mg)		Q (J)	ΔH (kJ mol^{-1})	ΔG (kJ mol^{-1})	ΔS (J mol^{-1} K^{-1})
Loading	2.50	–0.181	–42.64	97.63	–452.98
Release	1.32	0.069	10.30	–73.49	265.88

We chose equations 8 and 9 as the model functions that describe the drug-loading processes [37].

$$\frac{\mathrm{d}\alpha}{\mathrm{d}t}=kf(\alpha) \tag{8}$$

$$f(\alpha)=(1-\alpha)^n \tag{9}$$

where α is the degree of conversion at time t, $f(\alpha)$ is the kinetics function, and k is the reaction rate constant for the drug-loading process. Combining equations 8 and 9 yields the following:

$$\frac{d\alpha}{dt}=k(1-\alpha)^n \tag{10}$$

where H_t represents the enthalpy at time t and H_0 is the enthalpy of the whole process at time 0. Substituting $\alpha = H_t / H_0$ into the Eq. 10, we get

$$\ln[\frac{1}{H_0}(\frac{dH}{dt})_i]=\ln k+n\ln[1-(\frac{H_t}{H_0})_i] \qquad i=1,2,\cdots,L \tag{11}$$

where α is the conversion degree; $f(\alpha)$ is the kinetic function; H_t represents the heat at time of t; H_0 is the heat of the whole process; k is the reaction rate constant of drug-loading processes and n is the reaction order, L is the counting number. By substituting the experimental data into equation 8, we can draw a linear relationship

New Journal of Chemistry Accepted Manuscript

between $\ln[1-(\frac{H_t}{H_o})]$ and $\ln[\frac{1}{H_o}(\frac{dH}{dt})]$ (Fig. 8b). The slope represents the reaction order (n), and the intercept represents ln$k$. We obtained n =1.19, ln k = –8.43, and r = 0.9952 for this relationship. This result shows that the drug-loading processes are similar to quasi-first-order reactions. We can determine the kinetics equation for the drug-loading process: $\frac{d\alpha}{dt}=10^{-3.66}(1-a)^{1.01}$. This indicates that the reaction between the drug molecules and the nanocarriers is a simple reaction that occurs easily at a low temperature; that is, it is easy to load the drug.

3.5 Release of the drug upon microwave irradiation

Prior to applying microwaves as a stimulus to trigger the drug's release, we investigated the effect of microwave irradiation on the temperature increase in physiological saline solution with or without Fe_3O_4 (0.1 mg mL^{-1}) or Fe_3O_4@SnO_2:Er^{3+},Yb^{3+} (0.1 mg mL^{-1}) as a function of the irradiation time (Fig. 9a). The solution was irradiated with microwaves at 2.45 GHz and a power of 8 W for 20 min, which is within the range of values used for biomedical applications (2.45 GHz ± 0.05 GHz)[36]. The temperature of the Fe_3O_4@SnO_2:Er^{3+},Yb^{3+} solution increased to 319.55 K after 10 min. This temperature is known to be sufficiently high to release loaded drugs[11]. However, the temperatures of the physiological saline and Fe_3O_4 solution reached only 309.65 K and 303.95 K, respectively, after 10 min. These results showed that Fe_3O_4@SnO_2:Er^{3+},Yb^{3+} can quickly convert electromagnetic energy into thermal energy. Microwaves absorbed by the ferroelectric and dielectric Fe_3O_4@SnO_2:Er^{3+},Yb^{3+} nanoparticles will be converted into heat due to the loss of electrical energy, causing the temperature to rise. This shows that the as-prepared nanoparticles were suitable for localized heating to control drug release.

New Journal of Chemistry Accepted Manuscript

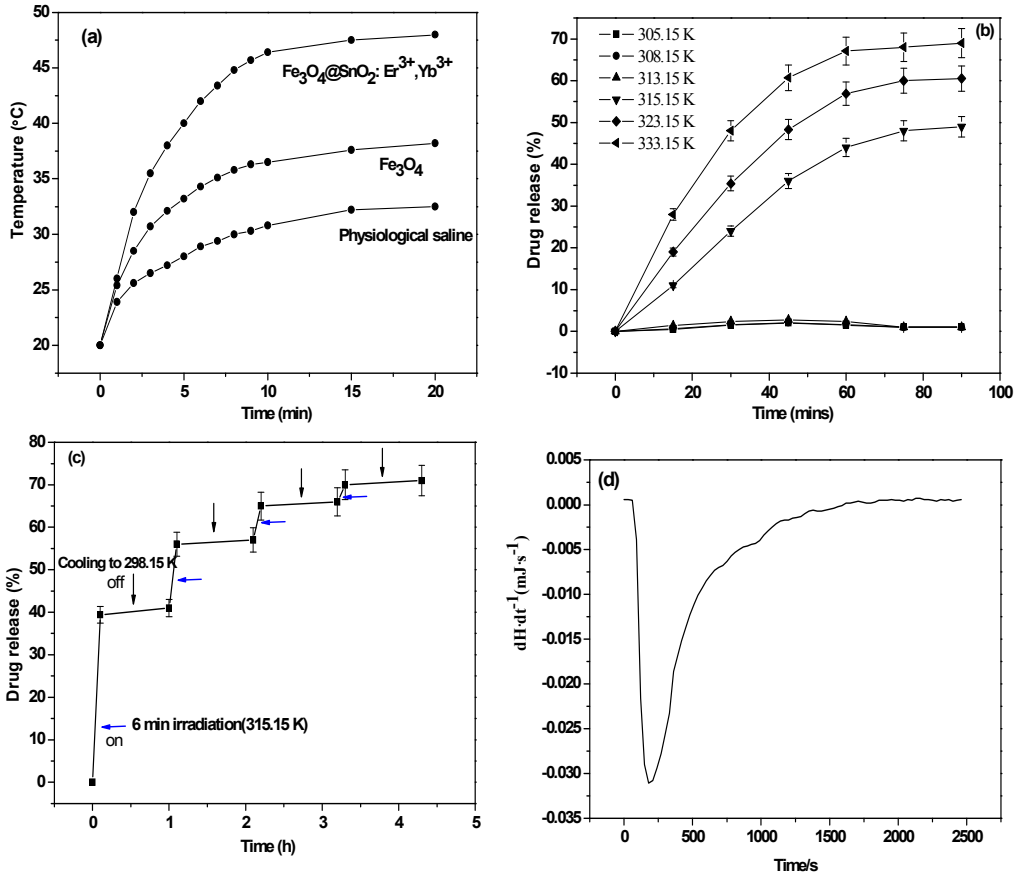

Fig. 9. (a) The heating curves for physiological saline solution, Fe_3O_4 solution (100 mg L^{-1}) and Fe_3O_4@SnO_2:Er^{3+},Yb^{3+} solution (100 mg L^{-1}) under microwave irradiation at 2.45 GHz and 8 W. (b) The drug release profiles for the release of ibuprofen from Fe_3O_4@SnO_2:Er^{3+},Yb^{3+}–APTES –ibuprofen (at 0.1 mg mL^{-1}) at six temperatures. (c) The controlled-release profile for Fe_3O_4@SnO_2:Er^{3+},Yb^{3+}–APTES–ibuprofen under microwave irradiation during four on/off cycles. Downward arrows indicate cooling periods; left-facing arrows indicate irradiation periods. (d) The endothermic curve for the drug release process.

We also investigated the effect of temperature on breaking of the hydrogen bonds between ibuprofen and Fe_3O_4@SnO_2:Er^{3+},Yb^{3+}–APTES. Fig. 9b shows that little to no drug release occurred at temperatures lower than 315.15 K. This demonstrates that the hydrogen bond between ibuprofen and Fe_3O_4@SnO_2:Er^{3+},Yb^{3+}–APTES remains stable at these temperatures. However, at temperatures ≥315.15 K, the drug release increased sharply within the first 90 min, suggesting that the hydrogen bond between ibuprofen and

New Journal of Chemistry Accepted Manuscript

Fe_3O_4@SnO_2:Er^{3+},Yb^{3+}–APTES broke at these temperatures. These results reveal that the hydrogen bond is sensitive to temperature and that the critical temperature for drug release is about 315.15 K. This also suggests that controlled drug release at biologically safe temperatures is possible. It also suggests that the nanocarrier will have good stability in circulation through the blood at normal body temperatures.

We determined the controlled release of ibuprofen from the Fe_3O_4@SnO_2:Er^{3+},Yb^{3+}–APTES–ibuprofen complex by microwave irradiation using UV-vis spectroscopic analysis. To evaluate the control and triggering mechanisms, we irradiated the nanoparticle solution with microwaves using four on/off cycles. For each cycle, the sample was irradiated for 6 min and then the microwave was turned off for 1 h (to allow cooling to 315.15 K). Fig. 9c shows that the ibuprofen concentration increases greatly during microwave irradiation, but that when the microwave is turned off, release of the drug molecules nearly stops. This suggests that the release of ibuprofen can be attributed to thermal effects induced by the microwaves, which break the hydrogen bonds. Approximately 71% of the ibuprofen was released after four cycles. When the microwave irradiation was turned off, the medium temperature decreased to below the temperature threshold required to break the hydrogen bonds and the hydrogen bonds remained sufficiently strong to retain the drug molecules. If this were not the case, the release would have been continuous even during cooling to 298.15 K. The results demonstrate that microwave irradiation can be used to control drug release from the Fe_3O_4@SnO_2:Er^{3+},Yb^{3+}–APTES nanocarriers and that the amount of the drug that is released can be controlled by modifying the irradiation duration and intensity.

Fig. 9d shows the thermodynamics of the drug release process at 315.15 K. From the abovementioned results, we know that the binding of the nanocarrier with the drug

New Journal of Chemistry Accepted Manuscript

is an exothermic process and that the main force is hydrogen bonding. Thus, when the drug is released from the nanocarrier, it must absorb heat from its environment to break the bonds. Fig. 9d shows that the enthalpy change is dramatic at the beginning of heating (about 25 min), which indicates a rapid drug release rate. After about 25 min, the rate of enthalpy change stabilizes near 0, which shows that the drug release rate decreases greatly. Thus, the time to reach equilibrium is about 25 min, drug release is a relatively fast process, and heating weakens the hydrogen bonds between the nanocarrier and the drug, thereby increasing the drug release rate. This is further evidence that the bonds between the nanocarrier and drug can be easily broken. Table 1 shows that the enthalpy change (ΔH) during the drug release process is 10.30 kJ mol^{-1}, which confirms that this is an endothermic process. This provides a simple method to monitor the drug loading and release processes and control drug release.

3.6 Cytotoxicity Assay

To evaluate the cytotoxicity of the nanocarrier and of the thermal effect induced by microwave irradiation, we performed an MTT assay using MCF-7 cells. The absorbance of MTT at 490 nm depends on the degree of activation of the cells. We expressed the cell viability as the ratio of absorbance by the treated cells (incubated with the nanoparticles or irradiated with microwaves) to that of the untreated cells. The nanocarrier produced almost no cytotoxicity or side-effects in living cells (Fig. 10a). The microwave irradiation and the associated thermal effects also produced no obvious decrease in cell viability (Fig. 10b), even after three irradiations; thus, microwave irradiation with a power of 8 W for 10 min caused little to no damage to the living cells. An additional advantage of our nanocarriers is that many cancer cells will die if they are exposed to a temperature of 315.65 K for more than 3 h, whereas normal cells can survive for a long time at 318.15 K[39].

New Journal of Chemistry Accepted Manuscript

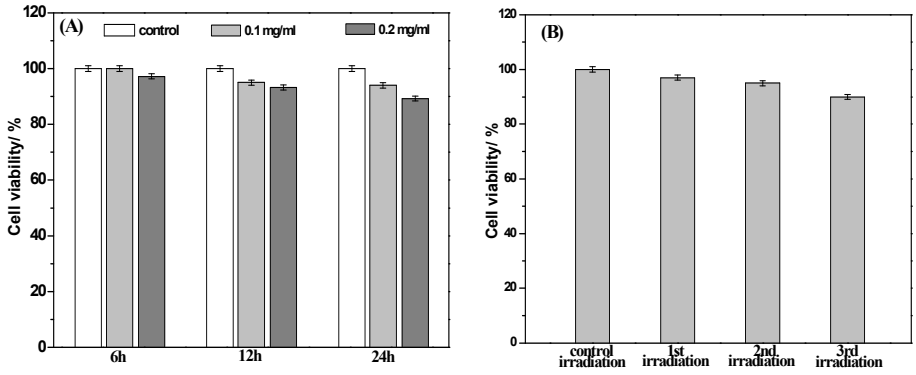

Fig. 10 (a) Viability of the MCF-7 cells incubated with different amounts of Fe_3O_4@SnO_2:Er^{3+},Yb^{3+}–APTES for different times. (b) Viability of the MCF-7 cells incubated with Fe_3O_4@SnO_2:Er^{3+},Yb^{3+}–APTES for different numbers of microwave on/off cycles.

4. Conclusions

In this study, we used the hydrothermal method to fabricate multifunctional core-shell structure Fe_3O_4@SnO_2:Er^{3+},Yb^{3+}–APTES nanoparticles with good magnetization and up-conversion luminescence properties. Thermodynamic assays showed that the interaction between the nanocarrier and the drug occurred through relatively weak hydrogen bonds, and that the bonds were easily broken by microwave irradiation. Ibuprofen released slowly to 2.0% at 60 min without microwave irradiation, and with microwave irradiation the release is improved to 38% at 6 min. Approximately 71% of the ibuprofen was released after four microwave on/off cycles. The MTT assay revealed that both the nanocarrier and the microwave irradiation produced little cytotoxicity and few side effects in the living cells. We anticipate that the insights provided by our study will lead to the design of new and more effective on-command drug delivery systems.

New Journal of Chemistry Accepted Manuscript

Acknowledgments

This work was supported by the National Natural Science Foundation of China (No. 21071115) and by the Innovative and Entrepreneurial Training Program for the National College Students (No. 201210697010).

References

[1] L. J. Zhu, D. L. Wang, X. Wei, J Control Release. 2013,**169**, 228.

[2] H. Y. Chen, D. Sulejmanovic, T. N. Moore, Chem Mater. 2014, **26**, 2105.

[3] H. Xu, L. Cheng, C. Wang, Biomaterials. 2011, **32**, 9364.

[4] T. M. Guardado-Alvarez, L. S. Devi, M. M. Russel, J Am Chem Soc. 2013, **135**, 15269.

[5] L. Cheng, K. Yang, Y. Li, Angew. Chem. Int. Ed. 2011, **50**, 7385.

[6] L. Li, C. Liu, L. Y. Zhang, Nanoscale. 2013, **5**, 2249.

[7] S. F. Lee, X. M. Zhu, Y. X. Wang, Am Chem Soc. Appl. Mater. Interfaces. 2013, **5**, 1566.

[8] A. Riedinger, P. Guardia, A. Curcio, Nano Lett. 2013, **13**, 2399.

[9] B. Liu, C. X. Li, P. A. Ma, Nanoscale, 2015, **7**, 1839

[10] Z. W. Li, C. Wang, L. Cheng. Biomaterials. 2013, **34**, 9160.

[11] C. R. Thomas, D. P. Ferris, J. H. Lee. J Am Chem Soc. 2010, **132**, 10623.

[12] R. J. Gui, A. J. Wan, X. F. Liu, Chem Commun. 2014, **50**, 1546.

[13] J. Cao, S. S. Huang, Y. Q. Chen, Biomaterials. 2013, **34**, 6272.

[14] N. Li, Z. Z. Yu, W. Pan, Adv Funct Mater. 2013, **23**, 2255.

[15] P. Lu, J. L. Zhang, Y. L. Liu and H. Jin, Talanta. 2010, **822**, 450.

[16] P. Sun, H. Y. Zhang, C. Liu, J. Fang, Langmuir. 2010, **262**, 1278.

[17] J. W. Liu, J. J. Cheng, J. J. Che, J Phys Chem C. 2013, **117**, 489.

[18] Y. J. Chen, P. Gao, R. X. Wang, J Phys Chem C. 2009, **113**, 10061.

[19] S. Lechevallier, P. Hammer, J. M. A. Caiut, Langmuir. 2012, **28**, 3962.

[20] S. Sharma, J. Shah ,R.K. Kotnala, Electronic Materials Letters, 2013, **9(5)**, 615-620.

[21] E.A. Morais, S.J.L. Ribeiro, L.V.A. Scalvi, J Alloy Compd. 2002, **344(1)**: 217–220.

[22] S. Y. Lee, C. Y. Ahn, J. Lee, and J. H. Chang, Talanta. 2012, **93**, 160.

[23] Y. L. Wang, B. X. Han, Langmuir. 1997, **13**, 3119.

New Journal of Chemistry Accepted Manuscript

[24] M. Indrajyoti, S. Diptabhas, S. P. Moulik, Langmuir. 2010, **26(23)**, 17906.

[25] W. G. Liu, X. C. Zhang, H. Y. Li, Composites: Part B. 2012, **43**, 2209.

[26] Q. Xiao, C. Xiao. Nanoscale Res Lett. 2009, **4**, 1078.

[27] H. Deng, X. L. Li, Q. Peng. Composites: Part B. 2012, **43**, 2209.

[28] S. H. Wang, R. Guo, L. F. Zheng. Nanotechnology. 2012, **23**, 105601.

[29] B. Feng, R. Y. Hong, L. S. Wang, Colloid Surf. A-Physicochem. Eng. Asp. 2008, **238(1-3)**, 52.

[30] J. Mohammad, I. A. R. Rahman, C. S. Sipaut, Synthetic Metals. 2012, **162 (6-7)**, 466.

[31] C. C. Tu, J. H. Hoo, K. F. Böhringer, Optics Lett. 2012, **37(22)**, 4771.

[32] M. Kokate, K. Garadkar, A. Gole, J Mater Chem A. 2013, **1**, 2022.

[33] N. Carreras, V. Acuña, M. J. Lis, Colloid Polym Sci. 2013, **291**, 157.

[34] X. Zhang, P. P. Yang, Y. L. Dai, and P. A. Ma, Adv Funct. Mater. 2013, **23**, 4067.

[35] Z. X. Li, W. W. Zhao, X. H. Pu, Thermochimica Acta. 2012, **537,** 76.

[36] P. D. Ross, S. Subramanian, Biochemistry.1981, **20(11)**, 3096.

[37] L. Xue, F. Zhao, X. Xing, and Z. M. Zhou, J Chem Eng Data. 2011, **56(2)**, 259.

[38] Y. M. Wang, Z. H. Luo, Mater. Lett. 2011, **65**, 3241.

[39] Y. J. Chen, P. Gao, G. G. Zhao, J Phys Chem C. 2009, **113**, 10061.

[40] K. Can, M. Ozmen, M. Ersoz, Colloids Surf. B. 2009, **71,** 154.

New Journal of Chemistry Accepted Manuscript

Table of Contents

New multifunctional core–shell nanocomposite were synthesized and applied as an efficient microwave sensitive nanocarrier for on-command drug release.

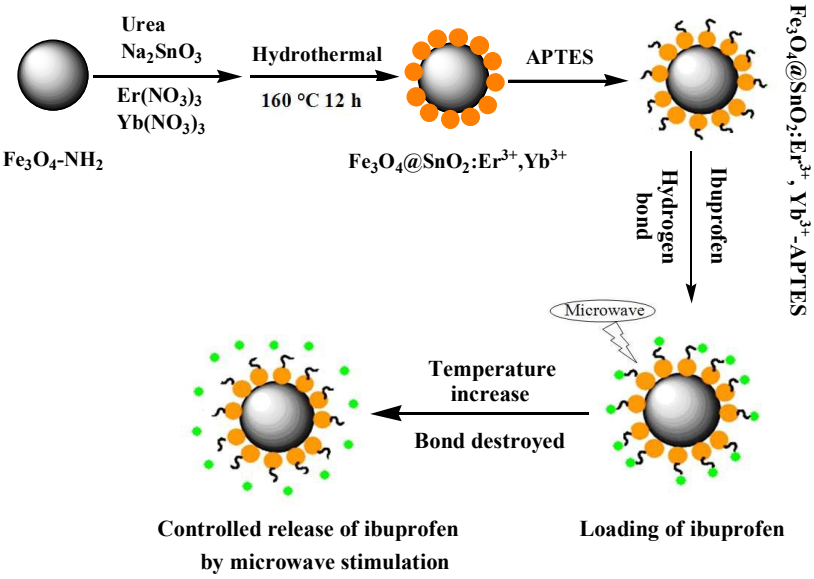

New Journal of Chemistry Accepted Manuscript